Available online at www.sciencedirect.com
SCIENCE DIRECT®
Journal of Nuclear Materials 327 (2004) 88–96
journal of nuclear materials
www.elsevier.com/locate/jnucmat

# He migration in implanted $UO_2$ sintered disks

S. Guilbert [a,*], T. Sauvage [a], P. Garcia [b], G. Carlot [b], M.-F. Barthe [a], P. Desgardin [a], G. Blondiaux [a], C. Corbel [c], J.P. Piron [b], J.-M. Gras [d]

[a] Centre d'Etudes et de Recherches par Irradiation (CERI), CNRS, 3A, Rue de la Ferollerie, Orléans 45071, France
[b] DEN/DEC/SESC/LLCC, CEA Cadarache 13115, France
[c] Laboratoire de Radiolyse, CEA Saclay 91191, France
[d] EDF/Research and Development Division, Les Renardières, Moret-sur-Loing 77250, France

Received 27 June 2003; accepted 23 January 2004

**Abstract**

The behaviour of helium implanted in sintered uranium dioxide disks has been investigated as a function of annealing temperature. $UO_2$ disks have been implanted with 1 MeV $^3He$ ions at a fluence of $1\times10^{16}$ $^3He\,cm^{-2}$ using a Van der Graaff accelerator. These implantation conditions lead to a local helium concentration of 0.2 at.% at a depth of 1.9 μm in $UO_2$. The $^3He(d,\alpha)^1H$ Nuclear Reaction Analysis method was used to determine the helium depth profile after the various annealing stages. The experimental results measured after 1100 °C anneal were analysed using a simple model which satisfactorily reproduces the observed helium depth profile changes. The intragranular helium diffusion coefficient is estimated and the result is assessed against other data published in the open literature.


*PACS:* 66.30.h; 61.82.m; 81.05.Je

## 1. Introduction

The release of fission gas, mostly Xe and Kr, from $UO_2$ and spent fuels has been extensively studied since the middle of the 1960s due to the potential effects on the structural and mechanical properties of the fuel [1–5]. Another rare gas that is produced in-pile, is helium, but a much greater quantity would be produced under long term storage by alpha decay of actinides especially in the case of MOX fuels: the volume of fission gas generated in-pile is around 2500 $cm^3$/rod STP – 1.5% at/$at_{iHM}$ [6,7]. For comparison, the amount of helium produced in MOX fuels after 10,000 years is evaluated at 6700 $cm^3$ STP per rod – which equates to 4% He atoms/initial heavy metal atoms at/$at_{iHM}$ – for a burnup of 47.5 GWd/tU.

In a previous paper [8], the behaviour of He was studied in sintered uranium dioxide disks in the 500–600 °C temperature range for a He content of 1 at.%. This previous study showed that He was not released at low temperature for annealing times of 1 h but that flaking due to He bubble precipitation occurred at temperatures as low as 500 °C.

In this paper, we present the experimental and modelling results obtained relative to the migration of helium in sintered uranium dioxide disks for lower He concentrations. Helium was introduced into the $UO_2$ disks by ion implantation. We used the $^3He(d,\alpha)^1H$ Nuclear Reaction Analysis method to determine the helium depth profile after post-implantation annealing from 600 up to 1100 °C. The experimental results measured after 1100 °C anneal were then analysed using a simple diffusion model which satisfactorily

* Corresponding author. Tel.: +33-2 38 25 54 29/27; fax: +33-2 38 63 02 71.
*E-mail address:* severine.guilbert@irsn.fr (S. Guilbert).

0022-3115/$ - see front matter © 2004 Elsevier B.V. All rights reserved.
doi:10.1016/j.jnucmat.2004.01.024

Table 1
Post-implantation annealing temperatures for each $UO_2$ disk

| Disk | First anneal $T$ (°C) | Second anneal $T + 300$ (°C) |
|---|---|---|
| E1 | – | – |
| E2 | 600 (1 h) | 900 (1 h) |
| E3 | 700 (1 h) | 1000 (1 h) |
| E4 | 800 (1 h) | 1100 (15 min) |

reproduces some of the observed helium depth profile changes.

## 2. Experimental

### 2.1. Sample preparation

Sintered uranium dioxide disks (0.2 at.% $^{235}U$) have been used for this study. The mean grain size is 8 μm and the mean O/U ratio determined by polarography is $2.0083 \pm 0.0060$. The density of the material is $10.46 \pm 0.03$ g cm$^{-3}$. The disks are 300 μm thick and 8.2 mm in diameter. After polishing of one side, the disks were annealed at 1300 °C in a $H_2$ atmosphere for 1 h to remove polishing damages (and to bring the samples back to a stoichiometric composition).

### 2.2. $^3He^+$ implantation

Four $UO_2$ disks (E1, E2, E3, E4) have been implanted with 1 MeV $^3$He ions using the 3.5 MV Van der Graaff accelerator at CERI Orléans. The implantation is performed by focusing the beam ($1 \times 1$ mm$^2$) and by sweeping it over the disk surface to ensure a homogeneous dose. The four disks of uranium dioxide were implanted during the same run at a nominal fluence of $1 \times 10^{16}$ $^3He^+$ cm$^{-2}$.

### 2.3. High temperature annealing under a $H_2$/Ar atmosphere

Anneals were performed under reducing atmosphere, 10 vol.% $H_2$/Ar, for 1 h. The atmosphere of the furnace was purged of oxygen before annealing by $H_2$/Ar sweeping for 1 h. The heating rate was approximately of 10 °C min$^{-1}$. The annealing lasted 1 h except for the anneal at 1100 °C which lasted only 15 min. At the end of the heating ramp, $H_2$/Ar was maintained in the furnace approximately 15 h during the cooling of the disks down to 30 °C in order to prevent oxidation of the disk surface. One disk was kept as-implanted (E1). The three other disks were annealed after implantation at a temperature in the 600–900 °C range. These temperatures are indicated in Table 1, column entitled 'first anneal'. The helium profile was measured by NRA and the disks were annealed a second time at $T + 300$ °C before a second NRA characterisation (Table 1).

### 2.4. Helium lateral and depth distribution

We used the $^3$He(d,α)$^1$H Nuclear Reaction Analysis method to determine the helium depth profile and lateral distribution in the first 3.5 μm under the surface. The measurements were performed at CERI Orléans with an

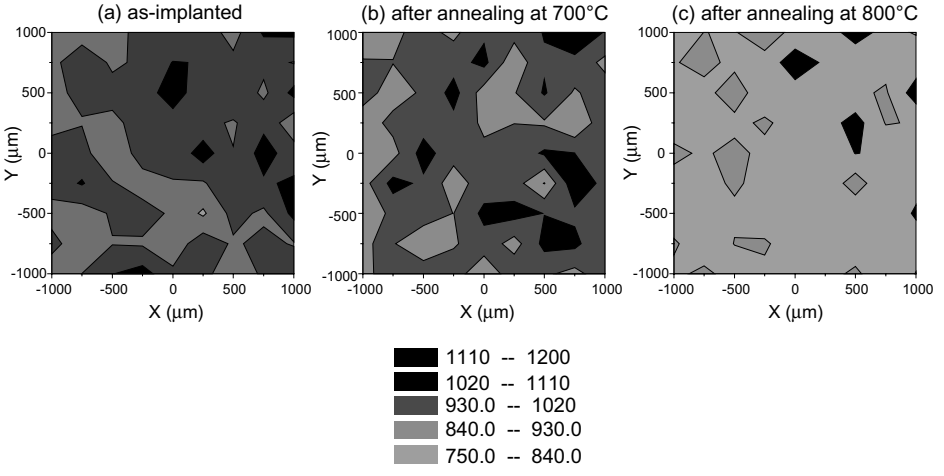


Fig. 1. Lateral helium distribution of implanted disk using proton detection (arbitrary units). The experimental data have been obtained by sweeping a $500 \times 500$ μm$^2$ deuteron beam on the surface of the samples with 250 μm steps in $X$ and $Y$ direction and plotted using contour mode. The gray scale at $X$, $Y$ position is defined by the value of $Z$ calculated by linear interpolation between the nearest values. (a) E1 as-implanted disk, (b) E3 implanted disk after annealing at 700 °C/1 h/$H_2$, (c) E4 implanted disk after annealing at 800 °C/1 h/$H_2$.

experimental set-up based on the detection in coincidence of both reaction products, α-particles and protons, at kinematically corresponding scattering angles. The helium profile is extracted from the alpha energy spectrum by using the reaction cross section and the energy-range relation for incoming and outgoing particles. The He lateral distribution is given by the proton yield detected in transmission geometry through the sample. To perform the lateral distribution measurements, the size of the deuteron beam was focussed to $500 \times 500$ μm$^2$. The proton yield was measured by sweeping the beam on the surface of the samples with 250 μm steps in the $X$ and $Y$ directions. The proton yield experimental values ($Z$) form matrix data which are plotted in Fig. 1 in contour graphs where ranges of $Z$ values are distinguished by different gray scale. The gray scale at $X$, $Y$ position is defined by the value of $Z$ calculated by linear interpolation between the nearest values.

The details of the method (experimental set-up, cross section data, energy calibration of the detectors and experimental data analysis) are described in [8,9].

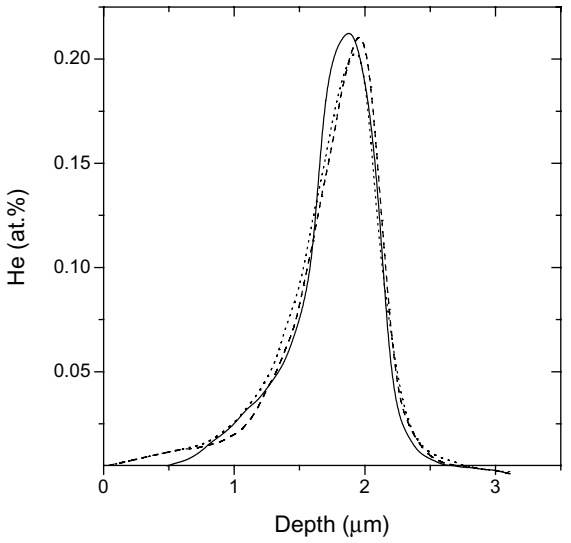


Fig. 2. Three experimental Helium depth profiles in as-implanted E1 disk (1 MeV, $10^{16}$ $^3$He cm$^{-2}$, $R_p = 2$ μm) determined using the $^3$He(d,α)$^1$H Nuclear Reaction Analysis.

## 3. Results

### 3.1. Lateral helium distribution

*After implantation*, as shown in Fig. 1(a), the helium lateral distribution, determined by NRA can be considered as homogeneous. The proton yield varies in the ±10% range around the mean value of 1042 counts for a total deuteron charge of 40 nC/point. The deviation to the mean value remains in the ±6% range for 95% of the sample surface as it can be expected for such statistic conditions.

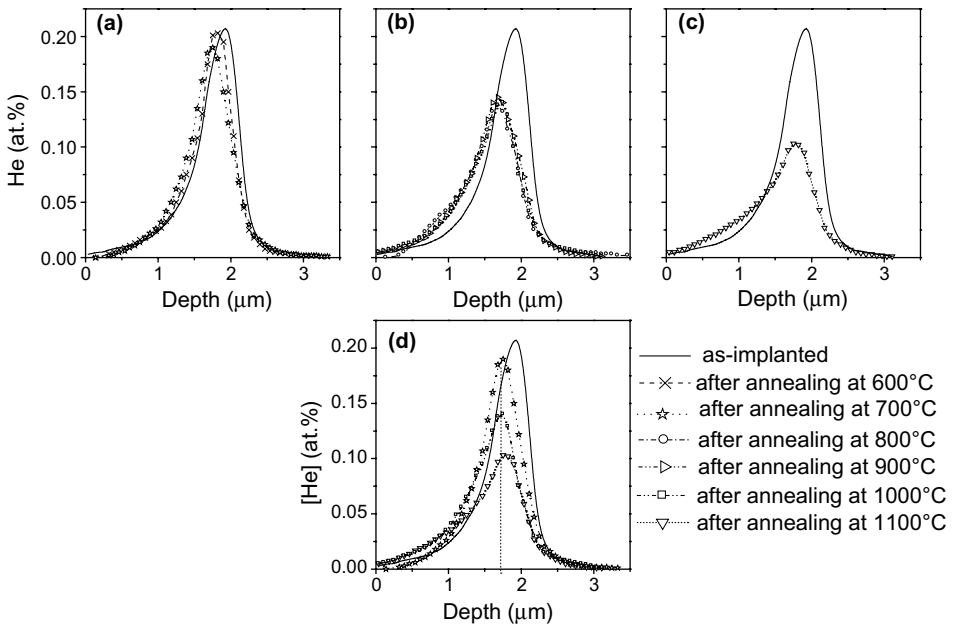


Fig. 3. He depth profiles in the as-implanted disk and (a) 600 and 700 °C annealed disks, (b) 800, 900 and 1000 °C annealed disks, (c) 1100 °C annealed disk, (d) 700, 1000 and 1100 °C annealed disks.

The helium lateral distribution was measured only after the first anneal of the E2, E3 and E4 disks.

*After annealing* at 600, 700 and 800 °C, the helium lateral distribution is homogeneous, as shown for 700 and 800 °C in Fig. 1(b) and (c) respectively. No flaking was observed, as it was the case at a higher fluence corresponding to a local helium concentration of 1% [8]. The mean proton yield is respectively $945 \pm 42$, $961 \pm 60$ and $805 \pm 42$ counts for a total deuteron charge of 40 nC/point. It is worth noting that the mean proton yield after annealing at 800 °C amounts roughly to ~80% of the mean proton yield measured on the as-implanted E1 disk.

### 3.2. Helium depth profile

#### 3.2.1. As-implanted disk

The He depth profile was measured in three different zones in the *as-implanted* disk E1 with a deuteron beam size of $500 \times 500$ μm$^2$. Fig. 2 shows that the He profiles measured on disk E1 are reproducible. The helium concentration reaches a maximum of $0.20 \pm 0.01$ at.%. This maximum is located at an average depth of $1.92 \pm 0.05$ μm and the average full width at half maximum (FWHM) of the He peak is equal to $0.57 \pm 0.03$ μm. The total helium content deduced from these profiles amounts to $(1.06 \pm 0.02) \times 10^{16}$ $^3$He cm$^{-2}$.

#### 3.2.2. Implanted and annealed disks

He depth profiles measured in implanted disks after annealing depend on the annealing temperature. Therefore, the results are presented according to three annealing temperature ranges.

*After annealing at* 600 and 700 °C, the helium profiles are very similar to the one measured in the as-implanted disk (see Fig. 3(a)). The maximum helium concentration is respectively equal to $0.20 \pm 0.01$ and $0.19 \pm 0.01$ at.%. The maximum helium concentration is detected respectively at $1.81 \pm 0.05$ and $1.73 \pm 0.04$ μm from the sample surface. The FWHM of the peak is respectively $0.56 \pm 0.03$ and $0.63 \pm 0.03$ μm and the total helium content amounts to $1.00 \times 10^{16}$ $^3$He cm$^{-2}$ for both anneals.

*After annealing at* 800, 900 and 1000 °C, Fig. 3(b) shows that the three helium depth profiles are alike. The maximum helium concentration is respectively equal to 0.135, 0.14 and 0.14 at.%. The maximum helium concentration is found respectively at a depth of 1.68, 1.68 and 1.73 μm and the FWHM is respectively equal to 0.76, 0.74 and 0.71 μm. The total helium content amounts to $0.87 \times 10^{16}$, $0.92 \times 10^{16}$ and $0.87 \times 10^{16}$ $^3$He cm$^{-2}$.

*After annealing at* 1100 °C for 15 min, the maximum helium concentration is equal to 0.1 at.% which is less than the value found after the 1000 °C anneal. This maximum is detected at 1.77 μm, and the FWHM is equal to 0.81 μm (Fig. 3(c)) and the total helium content amounts to $0.71 \times 10^{16}$ $^3$He cm$^{-2}$.

## 4. Discussion of experimental results

In this paragraph, the He profiles in as-implanted disks and their changes as a function of the annealing temperature are discussed.

*After implantation*, the 5.5% homogeneity in the He distribution is consistent with the method used to implant the disks. It is worth noting that the measured helium content, $(1.06 \pm 0.02) \times 10^{16}$ $^3$He cm$^{-2}$ is in good agreement with the implantation fluence, $10^{16}$ $^3$He cm$^{-2}$. The experimental depth corresponding to the maximum of the He content, $1.92 \pm 0.05$ μm, is in rather good agreement with the depth calculated using SRIM 2000 (2.08 μm). Nevertheless, the FWHM of the experimental $^3$He profile is larger than the one calculated using SRIM 2000, $0.57 \pm 0.03$ μm against 0.43 μm, and the maximum He concentration is 27% lower than the value obtained from SRIM calculations, $0.21 \pm 0.01$ at.% against 0.29 at.%.

As a function of annealing temperature, new features appear in the He profile pointing out a rearrangement of He atoms in the implanted disks.

*For annealing at* 600 and 700 °C, the maximum He content and the FWHM are similar to the ones obtained in the as-implanted disk E1 (Fig. 3(a)). No He release is observed for these annealing temperatures. However, a change in the depth corresponding to the maximum helium concentration and consequently in the He profile itself can be seen. The He peak shifts towards the surface as the annealing temperature increases: from about 100 nm at 600 °C to approximately 200 nm obtained after annealing at 700 °C. At 700 °C the shift percentage, calculated as the ratio of the shift value to the He peak position in the as-implanted disk, is 11%. The shift occurs with a slight broadening of the He distribution in the 700 °C annealed specimen in comparison to the as-implanted sample.

*For annealing at* 800 °C, a He peak shift of approximately 200 nm is still observed. The He distribution clearly broadens (+33%) as a result of the anneal. Moreover, the 800 °C anneal results in a He release of 18%. This release observed from disk E4 annealed at 800 °C, was obtained using a coincidence detection of the α and p particles and is in agreement with the low proton yield observed in the lateral distribution measured using proton detection. The proton yield in the E4 disk is 23% lower than the one determined in the E1 as-implanted disk.

*In specimens annealed at* 900 and 1000 °C, the He depth profiles are not significantly different from those obtained from the analysis of samples annealed at 800 °C. Furthermore, disks annealed at 800, 900 and 1000 °C show very similar helium release values (about 18%). After annealing at 1100 °C, a broadening of 42% of the He distribution is observed compared to the as-implanted E1 disk. The maximum He concentration is

located at the same depth than in the disk annealed at 800 °C. A decrease of the He maximum amount is noticed when compared to the one measured in the disks annealed at lower temperatures. Moreover, the He content which was 82% of the implanted fluence in disk E4 after the first anneal at 800 °C decreases to 67% after a 15 min anneal at 1100 °C. It follows that the total He release is 33% for the annealed disk E4.

To summarise experimental results, for annealing temperatures up to 700 °C, the *He profile shifts towards the surface*. *The observed shift in the maximum He concentration depth can represent* up to 11% of the as-implanted depth. *A first stage for He release* occurs at 800 °C. From 800 °C up to 1000 °C, there are no significant changes in the He concentration profiles. Finally at 1100 °C, a *second He release stage* is observed.

The He shift towards the surface suggests that He atoms are mobile at temperatures as low as 600 °C and are trapped at implantation induced defects as has already been observed in crystalline Si [10] and also in polycrystalline $MgAl_2O_4$ [11]. Corni et al. [10] observed a forward He profile shift of 45 nm in 20 keV helium-implanted silicon ($R_p = 215$ nm) after annealing. By correlating ERD, PAS and DC-XRD measurements, the authors ascribed this 14% shift to the interstitial helium movement and trapping in the vacancy-like defects produced by the implantation. A forward shift of the maximum helium concentration was also observed in polycrystalline $MgAl_2O_4$ implanted with 900 keV $^3He^+$ ions [11]. The authors ascribed this shift to helium trapping in pores.

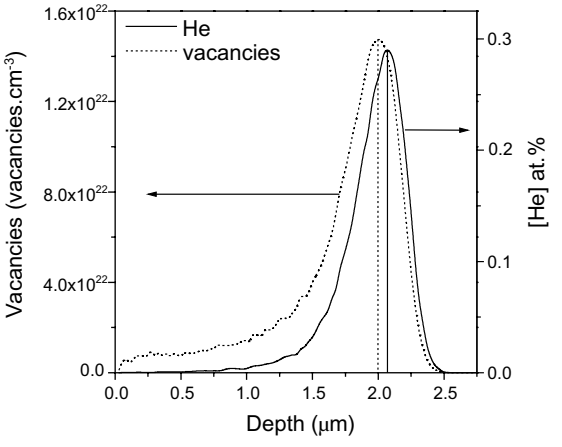


Fig. 4. SRIM 2000 calculations showing the distribution of 1 MeV $^3He^+$ in uranium dioxide and the total vacancy distribution along the helium path. A displacement energy of 40 eV for uranium and 20 eV for oxygen has been used [12].

We now discuss the role of He trapping at vacancy defects in the forward shift of the He depth profile observed after annealing in $UO_2$ sintered disks.

In Fig. 4, the distribution of the total vacancies and the He profile, calculated by SRIM 2000, for a 1 MeV $^3He$ implantation in $UO_2$ are shown. The calculated vacancy distribution is characterised by a peak with a maximum located at 2 μm, that is to say 80 nm before the calculated maximum He concentration. The relative positions of the helium and vacancy distributions support the assumption of He rearrangement in the cascade region and would explain the He peak shift towards the surface observed after annealing. The 80 nm theoretical difference is however lower than the actual peak shift observed after annealing (200 nm in this study).

There is also an experimental argument to support this assumption. Flaking has been observed in similar $UO_2$ sintered disks implanted with 1 MeV $^3He$ ions at doses 5 times greater and after annealing at 600 °C [8]. This flaking suggests that He bubbles are formed [13] at the depth which corresponds to the thickness of the observed flakes (i.e. ~1.6 μm). As it has been demonstrated in Si [10], one of the processes involved prior to He bubble formation is the He rearrangement in the high defect concentration region which occurs when the implanted samples are annealed. This would suggest that the vacancy defect profile in sintered $UO_2$ disks implanted with 1 MeV $^3He$ ions is indeed located at approximately 1.6 μm from the sample surface. This value is also comparable to the maximum He concentration depth determined in 1 MeV $^3He$ implanted $UO_2$ disks after annealing at 800 °C (1.68 μm). In conclusion, the He peak shift observed after annealing in the implanted $UO_2$ disks can be ascribed to He migration and trapping at vacancy defects created in the cascade region at a depth approximately 200 nm ahead of the maximum He concentration.

During this stage of migration, a small fraction of He, approximately 18% at the most, escapes the $UO_2$ disk at annealing temperatures of 800 °C.

At higher annealing temperatures (900 and 1000 °C), helium atoms appear to lose their mobility suggesting that trapping at bubbles that have nucleated at lower temperatures is still efficient.

During anneal at 1100 °C, helium atoms become mobile again, presumably because of thermal re-solution. Thermal re-solution is a phenomenon which for many years was held responsible for fission gas release observed in post-irradiation anneals (see for instance [14]). There appears nowadays to be a general consensus to the contrary, since many authors [15–17] have shown xenon or krypton solution or even incorporation energies in the uranium dioxide lattice to be relatively high. A solution energy is expressed as the sum of the incorporation energy, which corresponds to the energy

required to insert an atom in a pre-existing lattice defect, and the formation energy of the crystal defect in which the solute atom is inserted. Solution energies are therefore necessarily greater than incorporation energies. Recent ab initio calculations ([16] or [17]) estimate the lowest krypton incorporation energies, i.e. the energy needed to insert a krypton atom in one of the most favorable pre-existing crystal defect, in this case a uranium vacancy, to be in the 3–4 eV range in stoichiometric $UO_2$.

Helium on the other hand is a much 'smaller' atom and theoretical solution and incorporation energies are understandably much lower. Incorporation energies [17] associated with larger crystal defects are reported to be as low as $\sim -7$ eV in stoichiometric $UO_2$. Solution energies are even found to be negative which would point to helium being soluble to a certain extent. Both post-irradiation fuel rod puncturing results and infusion experiments [18,19] are an illustration of this. It is therefore reasonable to assume that, as the thermal energy of helium atoms trapped in bubbles increases, it can become sufficiently high for the atom to 'jump' into an adjacent crystal defect. A slightly different interpretation is to assume that the thermal energy at 1100 °C (i.e. $E = \frac{3}{2}k_bT \approx 0.18$ eV) corresponds to the solution energy of helium atoms in the sample or more probably, since crystal defects may still exist in the vicinity of helium bubbles, to an intermediate value between the incorporation and the solution energy. In Ref. [16], the incorporation energy of helium in stoichiometric $UO_2$ is quoted as having a value of 0.1 eV.

As the threshold temperature necessary for helium atoms to be incorporated in the crystal lattice is reached, bubbles no longer act as helium sinks but as helium sources.

## 5. Modelling the diffusion and release of He in $UO_2$ disks annealed at 1100 °C

This chapter concerns the modelling of the He diffusion and migration in the implanted $UO_2$ sintered disk annealed at 1100 °C, leading to He release. Two different models have been used to describe the diffusion and migration of He in $UO_2$ sintered disks. It is firstly shown that a simple diffusion model cannot be used to interpret the concentration profile change observed in the 1100 °C anneal. With a slightly more complex model taking into account direct release mechanisms and diffusion enhancement as a result of defects induced during the implantation stage, the comparison between the calculated and experimental He profiles is excellent. Finally the diffusion coefficient value determined by using this diffusion model is discussed.

### 5.1. Description of the models and results

The first idea that springs to mind is to model the concentration profile change observed as a result of the 1100 °C anneal using a simple diffusion model. This involves solving the following partial differential equation (Fick's second law):

$$\frac{\partial C(x,t)}{\partial t} = D\frac{\partial^2}{\partial x^2}(C(x,t)), \tag{1}$$

where $D$ is the diffusion coefficient at 1100 °C and $x$ the distance from the sample surface or depth. Initial conditions $C(x,0)$ are given by the experimentally determined helium profile following the 1000 °C anneal. The helium concentrations at the surface and at infinity are assumed to be zero. The modelling was performed using the Mathematica package [20]. Calculations were run for various values of $D$ and the differences between the calculated and experimental He profile indicated that the helium profile changes are clearly not the result of simple diffusion. A more complex model has to be used which takes into account the direct release mechanisms discussed in the following paragraphs and the spatial distribution of defects induced during the implantation stage.

If helium intergranular diffusion proceeds at a much greater rate than intragranular diffusion, then gas escape would essentially occur via grain boundaries. Release and subsequent changes of the concentration profiles would involve a two stage process in which helium first migrates to the grain boundaries whence release proceeds at a quasi instantaneous rate on the scale of the duration of the anneal. In order to model this by simply using a one-dimensional equation, we assume that, after the 1000 °C anneal, no helium is left at the grain boundary. Most of the helium is assumed to be contained in intragranular bubbles. As the threshold temperature for thermal re-solution is reached the gas atoms are restored to the matrix and the concentration difference between the grain interior and grain boundary drives the gas out of the matrix. The rate of gas loss to the grain boundary, which equates to a loss of gas from the sample, is as in most rate diffusion models which involve the loss of a diffusing species to a microstructural feature (e.g. bubbles) assumed to be proportional to the difference in gas concentrations within the grain and at the grain boundary. The loss rate is therefore given by the following expression:

$$k \cdot (C(x,t) - C_{\text{inter}}(x,t)), \tag{2}$$

which according to assumptions of instantaneous He release at grain boundaries (see discussion above) can be reduced to

$$k \cdot C(x,t). \tag{3}$$

Another possibly more straightforward explanation for this direct loss term could be the presence of pores and surface roughness at the sample surface. The profiles shown in Fig. 2 for instance are averaged over $500\times500$ square microns. This surface covers pitted areas where typically micron-sized pores emerge [8]. The integral helium concentration may be a function of depth only, but the local concentration is essentially three-dimensional (or at least two-dimensional) around the pore. When the sample is heated, it is reasonable to assume that helium atoms close to the 'sides' of the pores will be released by migrating directly to the pore surface. Again, assuming the boundary condition imposes zero concentration at the sample surface, then the loss rate proportional to the concentration gradient should in effect be proportional to the concentration further away from the pore. Fluctuations in the integral helium concentration around the pore should therefore appear if this interpretation is correct.

Taking into account the direct loss term, the equation describing the concentration profile evolution is written as

$$\frac{\partial C(x,t)}{\partial t}=\frac{\partial}{\partial x}\left(D(x)\frac{\partial}{\partial x}C(x,t)\right)-kC(x,t). \tag{4}$$

A first set of parametric calculations were run for various values of $D$ and $k$, initially taken to be uniform across the sample. No values of $D$ and $k$ were found to describe the concentration profile as a whole. In particular, it appears that over the short anneal period at 1100 °C, there is very little change in the tail end of the concentration profile. The use of constant values for $D$ and $k$ over the entire He profile leads to an overestimation of calculated concentration values in the region which lies between ~0.8 μm from the sample surface and the point at which the He profile peaks. It was therefore decided to introduce a spatial dependence for $D$ and $k$ which reflects the presence of defects created by the initial implantation.

Any diffusion coefficient derived from such modelling will therefore inevitably reflect the presence of oxygen, uranium or more complex vacancy clusters and would consequently have to be considered as an irradiation enhanced property.

Finally a set of calculations were run and $D$ and $k$ values were determined to fit the experimental profile as closely as possible. The best fit results are shown in Fig. 6 for $D$ and $k$ depth variations shown in Fig. 5 and the following maximum $D$ and $k$ values:

$$D_{\max}=6\times10^{-17}\ \mathrm{m^2\,s^{-1}},$$

$$K_{\max}=2.5\times10^{-4}\ \mathrm{s^{-1}}.$$

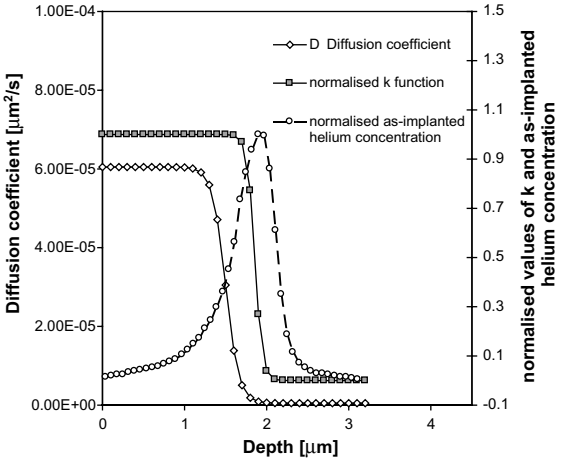


Fig. 5. Spatial variation of functions $D(x)$, $k(x)$ and experimental as-implanted 1 MeV $^3$He depth profile in $UO_2$ sintered disk, for annealing at 1100 °C.

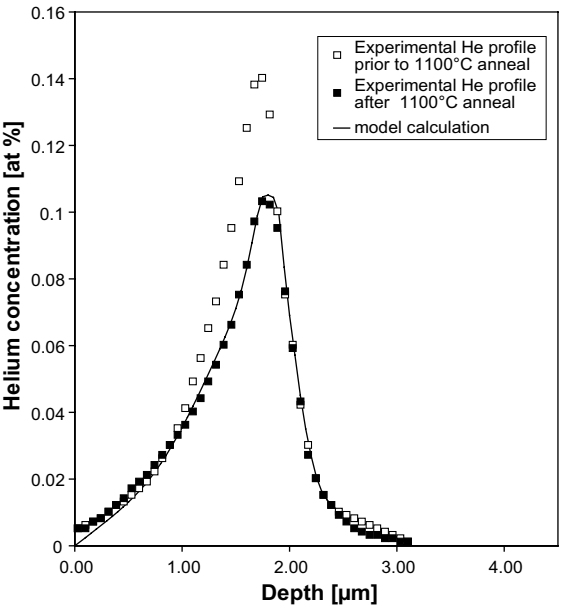


Fig. 6. Comparison of best-fit calculations and experimental data obtained in 1MeV $^3$He implanted $UO_2$ sintered disk, annealed at 1100 °C during 15 min.

The calculated and experimental data are clearly in good agreement.

It is also important to estimate the confidence one associates with the value of the diffusion coefficient derived from the modelling ($\sim6\times10^{-17}$ m$^2$ s$^{-1}$ at 1100 °C). To this end, calculations were run using $D_{\max}\times2$ and $\frac{D_{\max}}{2}$. Neither calculations are far removed from the best fit results. However, the corresponding profiles lie just

outside the ±5% uncertainty range associated with the concentration measurements. The diffusion coefficient can therefore be regarded as lying within a factor 2 of the diffusion coefficient which best fits the experimental results.

We have shown from numerical studies that the maximum values used for $D$ and $k$ are unique. It is quite possible however that different spatial distributions for the diffusion coefficient $D(x)$ and loss rate $k(x)$ exist, which could fit the experimental data equally well.

Having said that, the spatial dependencies for $D$ and $k$ applied to this study would indicate that as a result of the initial helium bombardment, vacancy defects are created in the region between the surface of the sample and the projected range of the incident ions. These defects would appear to efficiently assist the migration of helium.

### 5.2. Discussion

There is little data regarding the thermal diffusion properties of helium in $UO_2$. The only available data were derived from 'infusion experiments'. These experiments involve pressurising in a helium atmosphere a uranium dioxide sample at various temperatures and then after a given time, ascertaining the amount of helium trapped in the sample by dissolving it. The infusion results are then analysed using a time-dependent diffusion equation. The diffusion coefficient, assumed to be constant throughout the sample, and the concentration of the solute at equilibrium are then determined as those that best fit the dissolution results.

Rufeh et al. [18] thus obtained a diffusion coefficient ($1.5\times10^{-17}$ m$^2$ s$^{-1}$) four times lower than the one derived in the present study ($6\times10^{-17}$ m$^2$ s$^{-1}$) although their experiment was conducted at 1200 °C.

The results of Sung [19] are more complex to analyse. The authors inferred from experiments run at different helium partial pressures, a dependence of the diffusion coefficient on the hydrostatic pressure exerted on the sample. However, it is quite probable that bubble precipitation may have occurred in the set of tests run. In this case, using a simple diffusion model to interpret the experimental data will inevitably lead to an overestimation of the diffusion coefficient inferred. Notwithstanding this misgiving, the diffusion coefficient inferred (i.e. extrapolated from the temperature and pressure dependence) at ~1 atmosphere pressure and 1100 °C is over one order of magnitude ($1.2\times10^{-18}$ m$^2$ s$^{-1}$) below the diffusion coefficient found in the present study.

Both these results would confirm that the helium diffusion coefficient inferred from the present study is enhanced as a result of point defects introduced in the material during the initial helium implantation.

## 6. Conclusions

In this work, the behaviour of He in uranium dioxide after implantation and post-implantation annealing was investigated using nuclear reaction analysis ($^3$He(d,α)$^1$H). This study shows that helium moves in the implanted disks at temperatures as low as 600 °C. There appears to be combined bubble precipitation and intergranular diffusion (or some other means of direct gas release) at temperatures above 600 °C and below 1100 °C. As the temperature reaches 1100 °C, bubbles appear to act as helium sources and helium atoms appear to be restored to the matrix, presumably as a result of thermal resolution. A simple one-dimensional diffusion model provides a value of $\sim6\times10^{-17}$ m$^2$ s$^{-1}$ for the diffusion coefficient of helium at 1100 °C. A direct loss term has to be included in the model to fit the observed changes in the helium profiles. Two interpretations can be given for such a term. It is consistent with intergranular diffusion proceeding at a far greater rate than volume diffusion. It could also possibly be due to the presence of pores at the sample surface or more generally surface roughness whence direct gas release can proceed unhindered.

The value of the diffusion coefficient derived here is substantially greater than previous values obtained using 'infusion experiments'. This is assumed to be due to the presence of the point defects in the disk resulting of the initial helium implantation.

## Acknowledgements

The authors are grateful to the French electrical utility Électricité de France (EDF) and the Research Program on the long term Evolution of Spent Fuel waste Packages of the CEA (PRECCI) for their financial support.

## References

[1] W.F. Miekeley, F.W. Felix, J. Nucl. Mater. 42 (1972) 297.
[2] G.T. Lawrence, J. Nucl. Mater. 71 (1978) 195.
[3] P. Lösönen, J. Nucl. Mater. 280 (2000) 56.
[4] J.A. Turnbull, C.A. Friskney, J. Nucl. Mater. 71 (1978) 238.
[5] V.F. Chkuaseli, Hj. Matzke, J. Nucl. Mater. 223 (1995) 61.
[6] C. Poinssot, P. Toulhoat, J.-P. Piron, C. Cappelaere, L. Desgranges, J.M. Gras, in: ANS Annual Meeting, San Diego, USA, 4–8 June 2000.
[7] J.-P. Piron, M. Pelletier, J.C. Dumas, C. Poinssot, J.M. Gras, in: ASME ICEM'01 Conference, Bruges, Belgium, 30 September–4 October 2001.
[8] S. Guilbert, T. Sauvage, H. Erramli, M.-F. Barthe, P. Desgardin, G. Blondiaux, C. Corbel, J.P. Piron, J. Nucl. Mater. 321 (2003) 121.

[9] T. Sauvage, H. Erramli, S. Guilbert, L. Vincent, M.-F. Barthe, P. Desgardin, G. Blondiaux, C. Corbel, J.P. Piron, F. Labohm, A. Van Veen, J. Nucl. Mater., accepted for publication.
[10] F. Corni, G. Calzolari, S. Frabboni, C. Nobili, G. Ottaviani, R. Tonini, G.F. Cerofolini, D. Leone, M. Servidori, R.S. Brusa, G.P. Karwasz, N. Tiengo, A. Zecca, J. Appl. Phys. 85 (1999) 1401.
[11] E.A.C. Neeft, A. Van Veen, R.P.C. Schram, F. Labohm, Prog. Nucl. Energy 38 (2001) 287.
[12] J. Soulard, J. Nucl. Mater. 135 (1985) 190.
[13] F. Pászti, Nucl. Instrum. and Meth. B 62 (1992) 377.
[14] J.R. Matthews, G.J. Small, in: Proceedings of IAEA TCM on Water Reactor Fuel Element Computer Modelling in Steady State, Transient and Accident Conditions, Preston, Lancs, 18–22 September 1988.
[15] R.W. Grimes, Fundamental Aspects of Inert Gases in Solids, Plenum Press, New York, 1991, p. 415.
[16] J.-P. Crocombette, J. Nucl. Mater. 305 (2002) 29.
[17] T. Petit, M. Freyss, Ph. Garcia, P. Martin, M. Ripert, J.-P. Crocombette, F. Jollet, J. Nucl. Mater. 320 (2003) 133.
[18] F. Rufeh, D.R. Olander, T.H. Pigford, Nucl. Sci. Eng. 23 (1965) 335.
[19] P. Sung, Equilibrium Solubility and Diffusivity of Helium in Single Crystal Uranium Dioxide, University of Washington, Ann Arbor, USA, PhD, 1967.
[20] Wolfram Research. Available from <http://http:/www.wolfram.com/products/mathematica>.